BOLETIN DE LA SOCIEDAD ESPAÑOLA DE
Cerámica y Vidrio
www.elsevier.es/bsecv

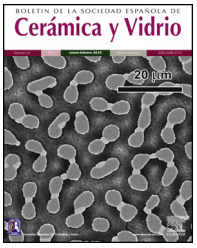

Calcium phosphate cements improved by addition of carbonated Hydroxyapatite type B

Jeisson Ruiz[a,1], *Daniel Moreno*[a,b,*,1], *Hamilton Copete*[a,b], *Fabio Vargas*[a,b], *María Esperanza López*[a,b]

[a] *Grupo de Investigación en Materiales y Recubrimientos Cerámicos GIMACYR, Universidad de Antioquia UdeA, Medellín, Colombia*
[b] *Grupo de Investigaciones Pirometalúrgicas y de Materiales GIPIMME, Universidad de Antioquia UdeA, Medellín, Colombia*

ARTICLE INFO

Article history:
Received 5 November 2021
Accepted 30 May 2022
Available online 10 June 2022

Keywords:
Tricalcium phosphate
Carbonate hydroxyapatite
Setting times
Mechanical properties
Calcium phosphate cements

ABSTRACT

The need for biodegradable bone graft biomaterials in orthopedic surgeries is more often each day due to the promotion of natural tissue regeneration. One option is calcium phosphate cements (CPC), that are also osseconductors. However, their low mechanical properties restrict their application to low mechanical requirement areas of the body. The CPC mechanical resistance depends on the entanglement grade of the calcium deficient hydroxyapatite (CDHA), one option to improve it is trough incorporation of nucleating agents (*e.g.,* stoichiometrically hydroxyapatite). This work proposes the use of a biodegradable nucleating agent, as it is Type B carbonated Hydroxyapatite (CHA-B), to improve the CPC performance. It was formulated compositions of alpha tricalcium phosphate (α-TCP) with variations on the amount of CHA-B (0–5–10–15 wt.%). The compression resistance was evaluated and results indicated that 5% CHA-B increases the strength (7.8%) and the elastic modulus (6.16%), while the other additions diminished such values. Besides, the effect on the setting time, the *in vitro* degradation and in the physicochemical properties was determined through scanning electron microscopy, X-ray diffraction and infrared spectroscopy.

Cementos de fosfato de calcio mejorados por la adicción de hidroxiapatita carbonatada tipo B

Palabras clave:
Fosfato tricálcico
Hidroxiapatita carbonatada
Tiempos de fraguado
Propiedades mecánicas
Cementos de fosfato de calcio

RESUMEN

La necesidad de biomateriales de relleno óseo biodegradables en cirugías ortopédicas es cada vez mayor, ya que promueven la regeneración natural del tejido. Una opción son los cementos de fosfato de calcio (CPC), que además son osteoconductores. Sin embargo, sus bajas propiedades mecánicas limitan su aplicación a zonas del cuerpo de baja exigencia mecánica. La resistencia mecánica de los CPC depende del grado de entrecruzamiento de los cristales formados de hidroxiapatita deficiente en calcio (CDHA), una opción de aumentarla

* *Corresponding author.*
E-mail address: daniel.morenod@udea.edu.co (D. Moreno).
[1] Authors contributed equally to this work.
https://doi.org/10.1016/j.bsecv.2022.05.002

es mediante la incorporación de agentes nucleantes (*e.g.* hidroxiapatita estequiométrica). Este trabajo propone el uso de un agente nucleante biodegradable, como lo es la Hidroxiapatita carbonatada tipo B (CHA-B), para mejorar el desempeño de los CPC. Se formularon composiciones de fosfato tricálcico alfa (α-TCP) con variaciones en la cantidad de CHA-B (0-5-10-15 wt.%). Se evaluó la resistencia a la compresión determinando que la adicción de 5% de CHA-B aumenta el esfuerzo (7,8%) y el módulo de elasticidad (6,16%), mientras que las demás adicciones disminuyeron dichos valores. Igualmente, se determinó el efecto en el tiempo de fraguado, en la degradación *in vitro* y en las propiedades fisicoquímicas mediante las técnicas de microscopía electrónica de barrido, difracción de rayos x y espectroscopía infrarroja.

Introduction

Calcium phosphate (CaP) bioceramics, also known as synthetic phosphocalcic apatites, have been widely used in the medical field for more than 40 years as bone substitutes to repair defects in this organ [1–3]. They share a great similarity in chemical composition for containing ions such as $H_2PO_4^-$, $H_2PO_4^{2-}$ or PO_4^{3-}, of which only the last two ions exist naturally in the mineral phase of the bones and teeth, giving them excellent biological properties for applications such as orthopedic and dental implants. In addition, they present physical properties similar to the mineral phase of natural bone [4,5].

Among the CaP, calcium phosphate cements (CPC) are known for being biocompatible and biodegradable making them good candidates to be used in orthopedic procedures. The use of bone grafting in surgeries have become frequent in traumatology and orthopedics, therefore there is a need to use materials that provide fast solution to the mechanical requirements, guarantee the well-being and increase life expectancy of the patients [6].

The precursors of CPCs are calcium orthophosphates, which form a family of chemical compounds that differ mainly in the calcium to phosphorous (Ca/P) molar ratio and in their water solubility. The most frequent used are: alpha and beta polymorphs of tricalcium phosphate (α-TCP and β-TCP), stoichiometric hydroxyapatite (HA) and carbonate hydroxyapatites type A, type B and type AB (CHA-A, CHA-B and CHA-AB, respectively) [7–9]. All of them present significant differences in their mechanical and biological properties, which allow to give specific use to each one according to the necessary application. However, nowadays α-TCP is one of the CaP that receives more attention as precursor of bone cements, due to its high solubility [10–13]. The high solubility leads to a faster dissolution and precipitation of calcium deficient hydroxyapatite (CDHA) that can directly influence the *in vivo* behavior of bioceramics, specifically in the degradation rate of the material at body conditions and the regeneration rate of the new bone [14].

CPCs are very important because at an *in vivo* level they present biodegradability and osteoconduction that help to integrate with the surrounding bone in the affected area and subsequently promote the bone regeneration [15]. CPCs are known for their versatility to graduate their injectiability and moldability by modifying the liquid-to-powder (L/P) ratio, however, they present low mechanical properties limiting their application to areas of the body with low mechanical requirements [16–20].

The mechanical resistance of CPCs is dependent on the degree of entanglement of the CDHA crystals. An option to increase it, is through the incorporation of nucleating agents as HA particles in a small percentages (3–10% w/w) [21]. HA is one of the most desired calcium phosphate for bone implants due to its hexagonal crystallographic system that provides greater stability. Such stability is linked to a low resorption kinetics, thus the material will not degrade in the body [22–24]. To increase resorption and to obtain a more suitable material for bone implants, there is the possibility of performing ion replacements in the HA that generate a distortion of this hexagonal structure, providing less stability, *i.e.*, greater solubility [2,25]. To achieve this, the hydroxyl ion (OH^-) or the phosphate ion (PO_4^{3-}) present in the HA can be replaced by a carbonate ion (CO_3^{2-}), this substitution can be carried out by physico-chemical means resulting in a carbonated hydroxyapatite (CHA) [23,25].

According to the position that CO_3^{2-} ion replaces in the HA, it will present a different denotation. In the case where the ion occupies the place of the OH^- ion, it is denoted as type A carbonate hydroxyapatite (CHA-A) and when it replaces the phosphate PO_4^{3-} ion, it is denoted as type B carbonate hydroxyapatite (CHA-B) [25,26]. The latter is the most common in natural bones and is the one used in this work as a nucleating agent for the CPC.

With the purpose to obtain a totally biodegradable CPC, including the nucleating agent, in this research it was elaborated a material composed of calcium phosphate cement - reinforced with type B carbonated hydroxyapatite (CHA-B) where different formulations were analyzed varying the addition of CHA-B as nucleating agent (0, 5, 10 and 15% in weight). The effect of addition of CHA-B to the physicochemical and mechanical properties and the *in vitro* performance of these CPC formulations based on α-TCP were evaluated.

Materials and methods

Synthesis of alpha tricalcium phosphate (α-TCP)

α-TCP was obtained following the protocol of previous works[11,27], briefly, a high temperature solid-state reaction of

calcium hydrogen phosphate ($CaHPO_4$, Alpha Aesar) and calcium carbonate ($CaCO_3$, Merck) at a 2:1 molar ratio was performed inside a furnace.

The mixture was heated to 1400 °C with 2 h hold and subsequent cooling to room temperature at 10 °C/min. Such cooling rate was demonstrated to be sufficient to retain and stabilize the desired alpha phase at room temperature [10,28]. The TCP was grinded in a centrifugal mill (S1000 Restch, Germany) using zirconia jar and balls of different diameters (197, 149, 101 mm ± 1 mm in diameter), this procedure was performed for 15 min at 500 RPM in order to decrease the particle size; finally, the particulate material was sieved through a # 500 (25 μm hole size) Tyler mesh. Passing material was used in the preparation of the cement specimens. Such milling process gives a coarse TCP with a mean particle size of 9.1 μm, a d_{10} of 1.5 μm and a d_{90} of 26.1 μm, as previously reported [11].

Synthesis of carbonate hydroxyapatite type B (CHA-B)

The CHA-B was obtained via inverse aqueous reactions of two solutions, the first, a calcium solution ($Ca(NO_3)_2$) that was deposited in a reactor with constant agitation, after a complete dissolution of the calcium precursor was observed, the reactor was submerged in a silicon water bath in order to obtain a better temperature control; this system is heated in an inert atmosphere to avoid the carbonation of the apatites, due to the carbon dioxide in the atmosphere. Once the system reached 95 °C, the second solution containing the $(NH_4)HCO_3$ and $(NH_4)_2HPO_4$ chemical compounds was added. The speed of addition of the solution was approximately of 10 mL/min, which guaranteed a slow flow avoiding the formation of calcite in the precipitate, besides it modulates the particle size of the precipitated CHA-B [25,26].

As the second solution is added, the maturation time starts, which consists in keeping the same system conditions for 30 min and controlling the precipitate pH in a range of 8–9 in order to avoid the appearance of hydrogen phosphate ions during CHA-B precipitation. Later, when the precipitates were obtained, filtration and washing with deionized water was performed to eliminate the remaining dissolved ions from the liquid phase of the reaction, as well as the ions adsorbed by the surface of the obtained precipitates. Finally, a drying process was carried out around 100 °C to eliminate the absorbed surface water and later a thermal treatment was carried out for 2 h at 400 °C, as the aqueous precipitation method tends to store a considerable amount of interlaminar water and residues of the precursor solutions during the synthesis [25,26].

Calcium phosphate cements preparation

CPCs were obtained by mixing α-TCP precursor with distilled water and CHA-B. Four different CHA-B additions (0–5–10 and 15% by weight) were performed and cements were noted as function of this addition as C0, C5, C10 and C15, respectively. All CPCs were obtained at an L/P ratio of 0.44 mL/g.

Prior to the cement preparation, CHA-B was treated to diminish agglomeration due to its nanometric particle size characteristic. An ethanol dispersion process was implemented by sonication for 30 min, then drying the CHA-B in an oven at 70 °C for about 2 h to evaporate the solvent and finally sieving through a #325 (44 μm hole size) Tyler mesh.

To obtain the cement, first the two solid components (α-TCP and CHA-B) were manually and vigorously homogenized for 1 min with the corresponding amount of distilled water to obtain the required L/P ratio. Afterwards, the molding was performed using the specific mold for each test. The molding time was as short as possible to control the setting, avoiding that the paste dries out and a heterogeneous consolidation of the sample occurred. For this purpose, for axial compression test, Teflon cylindrical molds were used in accordance to ASTM C1424 standard [29]. For diametral tension test, Teflon cylindrical molds were used based on reported by Baudin et al. [30].

The setting process was carried out mimicking body conditions, molds were placed inside an incubator at 37 °C (Incubator 1000, Heidolph Instruments). The process consisted of two stages, in the first one it was set in high humidity conditions (close to 100%) for 16 h to avoid swelling of the samples. In the second stage, the samples were completely immersed in a 0.9% weight/volume sodium chloride (NaCl) solution for 7 days.

Physicochemical characterization

Cement precursors

The physicochemical characterization of the cement precursors (α-TCP and CHA-B) in their powder state were done using the same characterization equipment. To identify the chemical elements and to determine the Ca/P molar ratio, samples were analyzed by means of dispersive wavelength X-ray fluorescence (WD-XRF) in a spectrometer using Rhodium (Rh) source (ARL Optim'X, Thermo Scientific).

A combustion analyzer (CS844, Leco) was implemented to identify the carbon content and thus estimate the carbonate present in the synthesized CHA-B.

Fourier transform infrared spectroscopy using attenuated total reflectance system (FTIR-ATR, PelkinElmer) was used to identify the characteristic chemical bonds in the wavelength range of 1600–400 cm^{-1} and 4000–450 cm^{-1} for α-TCP and CHA-B, respectively.

X-ray diffraction (XRD, EMPYREAN, PANalytical) with a copper radiation source (Cu kα, λ = 1.540598 Å) at 45 kV and 40 mA was used for the identification of the crystallographic phases, analyzed in the 2θ range of 20° to 60° with a step size of 0.02°. JCPDS files used for XRD phase identification were 09-0348 for α-TCP; 09-0169 for β-TCP and 9-432 for HA. High vacuum scanning electron microscopy (SEM, JSM 6490 LV, JOEL) was used to determine the morphology of the starting materials.

Calcium phosphate cements

The obtained cements with 0, 5, 10 and 15 wt.% additions of CHA-B were characterized after the setting process. Nevertheless, the final setting time was evaluated by a Vicat needle penetration test (63-L0028, Controls), following a modified protocol based on ASTM C191-18 [31]. This equipment has a removable steel needle with an approximate length of 50 mm and a constant cross section of 1.00 ± 0.05 mm in diameter. The test was carried out inside an incubator (Incubator 1000, Heidolph Instruments), where 37 °C temperature and

high humidity were controlled during setting. Modification of the protocol was as follows: molds of 12 mm of diameter and 6 mm of height were used. After an initial time of 30 min indentations were performed, a maximum of 5 indentation per mold were done to guarantee a minimum distance of 2.0 mm between indentations. For a single condition, several molds were used. The time and depth in millimeters of each penetration was registered until obtaining an indentation smaller than one millimeter as specified in the ASTM standard. This test was performed triplicated for each CPC condition.

In addition, the pH of the cements was monitored with a pH-meter (MP 220, Mettler Toledo) during the first 6 h of the hydration reaction and after 48 h to check the pH of stabilization. Protocol was stablished based on several researches [32–34], each cement condition was prepared as a slurry with a L/P ratio of 20 mL/g, continuously stirred and maintained at 37 °C. The high L/P and continuous agitation were applied to maintain the particles disperse avoiding sedimentation and to protect the membrane of the pH electrode.

WD-XRF was performed to identify any effect of the CHA-B addition on the final Ca/P molar ratio of the CPCs. Likewise, XRD was performed to identify differences among CPCs. For this purpose, phases were identified and quantified by Rietveld refinement using the materials analysis using free diffraction software (MAUD, University of Trento, Italy); the results were confirmed with a residual in weight percentage (Rwp) lower than 10% and a significance level equal or lower than 0.02 [35]. In addition to the JCPD files used for reagents identification, File # 46-905 was used to identify and quantify CDHA phase.

FTIR-ATR was performed in the wavelength range of 4000–450 cm^{-1}, analysis between 1600 and 400 cm^{-1} was performed to identify the phosphate bonds related peaks and above 3000 cm^{-1} to identify the OH^- peak related to the formation of an apatite in the CPC.

SEM images of each CPC were taken to analyze the influence of CHA-B addition on the microstructure after setting for 7 days.

Mechanical characterization

The cements produced were mechanically characterized by axial compression following the procedure described in ASTM C1424 [29], using a universal testing machine (AGS-X, Shimadzu) with a 50 kN load cell, the test was performed at a speed of 0.5 mm/min. Based on the engineering stress–strain curves calculated from the displacement–load curves and the specimen dimensions, the maximum stress value was determined. For each cement condition, five samples of 6.3 mm diameter and 12.7 mm height were analyzed.

The tensile strength of the cements was determined by means of the diametrical disk compression test based on the experimental results presented by Baudin et al. [30]. Samples of 6 mm diameter and 3 mm height were loaded at a speed of 1 mm/min. The tensile strength of the cements Eq. (1), was calculated according to the specimen's dimensions and the maximum force reached in the force-displacement curve.

$$\sigma = \frac{2F}{\pi D t} \tag{1}$$

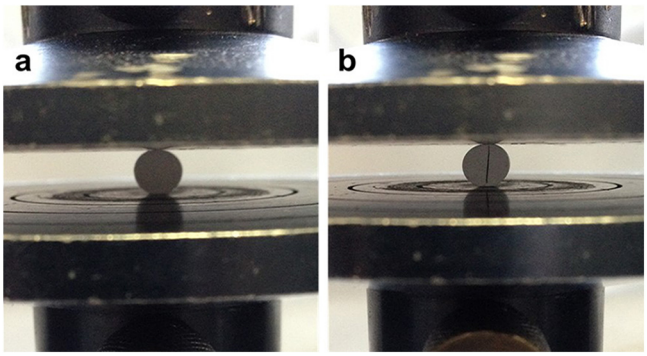

Fig. 1 – Mounting for diametric compression test (a). Characteristic fracture to validate the test (b).

where σ is the tensile strength, F the maximum force recorded in the force–displacement curve, D the diameter of the specimen and t the height of the specimen. Fig. 1a shows the assembly for the diametric compression test where it should be noted that, for the validity of this, the test must have a linear fracture along the center of the orthogonal plane to the applied force as shown in Fig. 1b.

A Weibull distribution analysis was applied to 15 valid results of each tested condition. After the test, specimens were used to analyze the fracture surfaces by SEM.

To plot the experimental values, the probabilities of failure were calculated from Eq. (2).

$$p_{f_i} = \frac{i - 0.5}{N} \tag{2}$$

where p_{f_i} are the Weibull distribution parameters, N is the total number of samples and i the samples organized in ascending order. Eq. (3) was used to calculate the cumulative distributions.

$$p_f(\sigma) = 1 - \exp\left(-\left(\frac{\sigma}{\sigma_0}\right)^m\right) \tag{3}$$

where $P_f(\sigma)$ is the probability of failure at a strength σ, m is the Weibull module and σ_0 is the characteristic strength.

In vitro testing

A quantitative comparison of the cements was performed based on the degradation study of calcium phosphates by Diez-Escudero et al. [36], an accelerated degradation test was performed by immersing the cements in an acid solution (pH 2.0), composed of 0.01 M hydrochloric acid and 0.14 M sodium chloride, test was performed inside an incubator at 37 °C and with constant agitation of 100 RPM. Before the test, the samples were dried at 100 °C for 12 h and their weight was recorded until a constant value was reached. The samples were immersed in 5.0 mL of the acid solution and this was renewed every hour to prevent changes in the pH of the solution, which could alter the degradation behavior. After 8 h of testing, the samples were washed with distilled water and dried at 100 °C until reaching a constant weight. For each

Table 1 – Percentage and molar content of Ca and P, Ca/P molar ratio of each precursor and carbonate content of CHA-B.

Precursor	Quantity	Ca	P	Ca/P ratio	Carbonate content (wt.%)
α-TCP	% Weight	38.33	19.88	1.49	–
	Moles	0.96	0.64		
CHA-B	% Weight	41.15	18.48	1.73	5.9
	Moles	1.03	0.60		

condition, 3 replicates were evaluated and finally the difference in weight was calculated according to Eq. (4).

$$\text{Mass loss} = \frac{m_i - m_f}{m_i} \times 100 \quad (4)$$

where m_i is the initial mass of the specimen and m_f is the final dry mass of specimen after the test. On the other hand, the pH of each one of the solutions was measured every hour, where it was obtained that it fluctuated between values of 1.97 and 2.03 in the pH scale; indicating that during the 8 h of test, the acidity of the solution was kept constant.

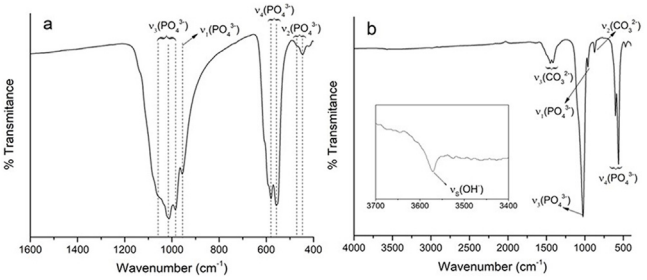

Fig. 2 – FTIR spectra. Alpha tricalcium phosphate (a), carbonate hydroxyapatite type B (b).

Results and discussion

Physicochemical characterization of precursors (α-TCP and CHA-B)

XRF and carbonate content

Table 1 shows the XRF results of the elements of interest, their equivalence in moles and the Ca/P molar ratio for each of the precursors and the carbonate content estimated in the CHA-B.

The theoretical Ca/P molar ratio for α-TCP is approximately 1.5, an appropriate value for this type of calcium phosphate. In the case of CHA-B, a Ca/P ratio equal to 1.73 is obtained, which is higher than the usual 1.67 presented by stoichiometric hydroxyapatite (HA). This increase is related to replacement of phosphate ions by carbonate ions during the CHA-B formation process, thus, the P decrease in the sample, leads to an increase in the Ca/P molar ratio, this is corroborated by the 5.9 wt.% carbonate content identified in the CHA-B, which agrees with reported in similar synthesis [37]. The approximately 1.5 Ca/P values obtained from the precursors give an indication of appropriate values for the biological processes that occur in the human body such as: adhesion and differentiation of bone cells, which are expected to be maintained in the derived obtained cements [10,12].

FTIR

The spectrum obtained by FTIR–ATR for the α-TCP, shown in Fig. 2a, presents four characteristic vibration modes of the phosphate ion (PO_4^{3-}): ν_1 at 956 cm^{-1} for symmetrical P–O stretching, ν_2 at 415–470 cm^{-1} for symmetrical double degenerated P–O rolling, ν_3 at 984–1058 cm^{-1} for antisymmetrical triple degenerated P–O stretching and ν_4 at 551–613 cm^{-1} for antisymmetrical triple degenerated P–O rolling [10,11].

The spectrum of CHA-B shown in Fig. 2b presents three modes of vibration characteristic of the PO_4^{3-} ion: ν_1 at 960 cm^{-1} for the symmetrical stretching of P–O, ν_3 at 1024 cm^{-1} for the triple degenerated antisymmetrical stretching of P–O and ν_4 at 551–613 cm^{-1} for the triple degenerated antisymmetrical stretching of P–O; in addition, two types of vibrations are presented for the CO_3^{2-} ion: ν_2 at 874 cm^{-1} and ν_3 at 1412–1456 cm^{-1} corresponding to the antisymmetrical stretching vibration of C-O. ν_2 and ν_3 vibrations of CO_3^{2-} ion are important to identify the type of substitution obtained in the HA as vibrations are present at different wavelengths. For type A substitution ν_2 is present at 878 cm^{-1} and ν_3 doublet at 1465–1542 cm^{-1}, and for type B they can be found at 872 cm^{-1} and at 1412–1462 cm^{-1} [38]. Thus, this result seems to indicate that type B substitution is being accomplished during the synthesis. Finally, a weak peak is observed at 3572 cm^{-1} for the stretching (ν_s) corresponding to the hydroxyl group, characteristic of hydroxyapatites [10,39], which confirms that although the substitution of ions has been made it remains to be a hydroxyapatite.

XRD and morphology of precursors

In the diffractogram of α-TCP reported in Fig. 3a, the identified peaks are mainly related to α-TCP phase and only one is related to the β-TCP phase, according to the patterns JCPD 9-348 and JCPD 9-169 respectively. This result corroborates that the heat treatment used in the synthesis is appropriate to obtain a tricalcium phosphate with a high content of the alpha phase with few impurities of the beta phase. As stated in other works, the beta phase trace is more related with the small content of beta stabilizers as magnesium (Mg) and strontium (Sr) [40,41], than with the cooling method to retain the alpha polymorph [11].

Fig. 3b shows the diffractogram of the CHA-B, which was contrasted with the JCPD 9-432 standard and it was obtained that all the peaks presented correspond to hydroxyapatite. Unlike stoichiometric HA, in the CHA-B spectrum the identified peaks are less defined and with a wider base, due to the incorporation of carbonate in its structure that distorts the hexagonal structure of stoichiometric HA, hinting that the obtained CHA-B is less crystalline and more reactive [39].

Fig. 3c corresponds to morphology of α-TCP, it is possible to observe particles of different sizes with irregular non-equiaxial characteristics and rounded tips, related to the

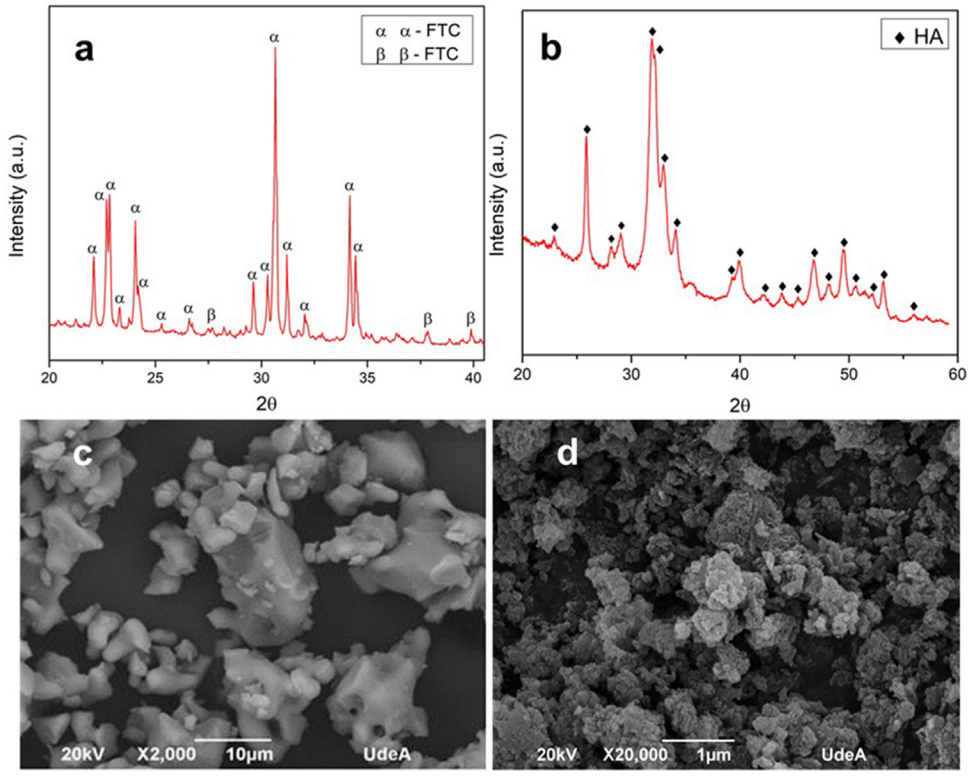

Fig. 3 – XRD from α-TCP (a). XRD from CHA-B (b). SEM micrograph from α-TCP (c). SEM micrograph of CHA-B (d).

Table 2 – Final setting time using the Vicat needle.

Cement	C0	C5	C10	C15
Final setting time (min:s)	219:97	194:82	173:99	128:28
Deviation	5:71	3:81	3:91	2:75

milling process, particles size ranges from 1.8 to 17.8 nm, which are inside the range determined in previous publication. Such particle size may be classified as a coarse TCP which will lead to a CDHA with plate-like morphology [19,42]. CHA-B is presented in Fig. 3d, where a large number of agglomerates is observed due to its hygroscopic nature and the nanometric scale of the particles of the material after the wet synthesis process.

Physicochemical, mechanical and *in vitro* characterization of calcium phosphate cements

Final setting time and pH evolution

Table 2 shows the final setting times determined by resistance to Vicat needle indentation. The final setting times obtained are 219:97 min:s, 194:82 min:s, 173:98 min:s and 128:29 min:s for conditions C0–C5–C10 and C15 by weight respectively of CHA-B content. The times obtained show that the greater the amount of CHA-B in the CPC, the shorter the final setting time, which can be attributed to the process of dissolution and precipitation that occurs during the setting time, this is evidenced by a drier and more difficult to mold paste as the addition of CHA-B is greater. This result corroborates that CHA-B addition acts as a nucleating agent that diminishes the setting time, effect that is known to be promoted when stoichiometric HA is added in the formulation of CPCs [43,44].

The obtained results are almost three times higher than final setting time values reported in literature of similar calcium phosphate cements, such difference is related to the temperature and humidity conditions that were controlled during setting in this work. Most setting time studies do not describe the conditions of these parameters (especially humidity) or in some cases are only reported to have been performed at room or body temperature [45–47]. The control of parameters such as temperature and humidity are of utmost importance when dealing with a material that can be used as a bone implant and its analysis should be carried out as close as possible to the conditions of use. The performance at high humidity allows the process of dissolution and precipitation, that occurs during setting, to be more controlled, preventing the material from cracking due to fast drying of the sample.

Fig. 4 shows the evolution of the pH slurry during the hydration reaction of each of cements formulated. As observed, the pH changed in the range values of 6.5 and 9.0 for all conditions, which suggest that the final cements will be of the apatitic kind as values are in the stability range of CDHA ($pH \geq 4.2$) and not in the one of brushite cements ($pH \leq 4.2$) [21]. In C0 it can be observed the behavior of α-TCP when mixed with water, the pH is increased to a maximum of 8.84 after 30 min of reaction, due to the basic character of the phosphate ion that is being release during the dissolution stage of the cement consolidation, afterwards the pH rapidly diminishes to a pH close to 8.5 and then at a minor rate toward a neutral pH. It is notorious that higher addition of CHA-B diminishes the maximum pH value and the time to reach it is faster. C5 reach a pH of

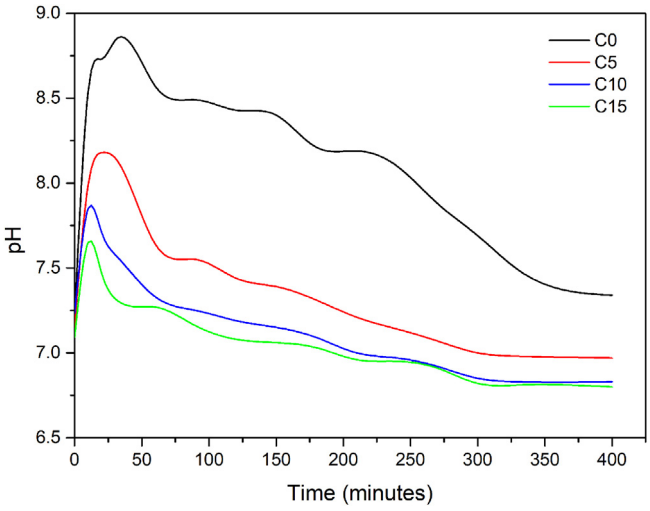

Fig. 4 – pH evolution of the cement formulations during the hydration reaction.

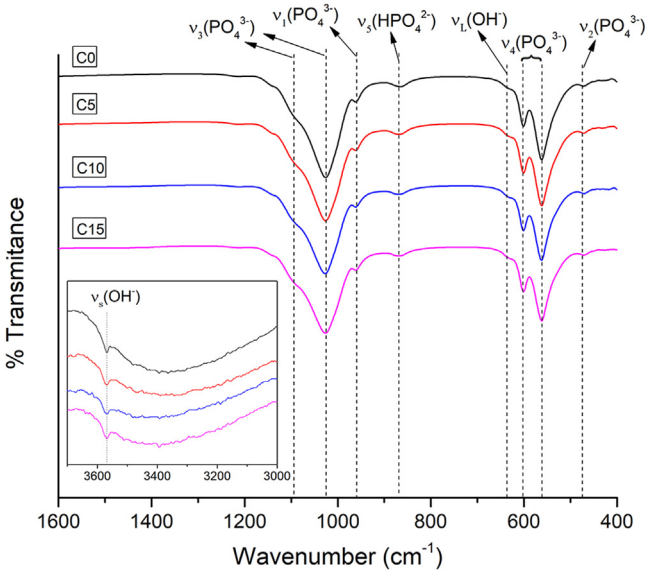

Fig. 5 – FTIR spectra of CPCs as a function of the percentage of CHA-B added. Insert for analysis between 3700 and 3000 cm^{-1}.

Table 3 – Elemental composition of CPCs and their Ca/P molar ratio.

Quantity	Ca	P	Ca/P molar ratio	Cement formulation
% weight	35.9	18.96	1.47	C0
Moles	0.9	0.61		
% weight	35.98	19.09	1.46	C5
Moles	0.9	0.62		
% weight	36.19	18.97	1.48	C10
Moles	0.91	0.61		
% weight	35.68	19.14	1.44	C15
Moles	0.89	0.62		

8.18 at 20 min, C10 a pH of 7.85 at 10 min and C15 a pH of 7.65 also after 10 min of reaction. The lower maximum pH values are attributed to the acidic character of the carbonate ion, however, it is corroborated that the phosphate basic character maintains the slurry in the appropriate range for precipitation of CDHA crystals. The shortening in time to reach such maximum is suggesting that the addition of HAC-B is in fact acting as a nucleating agent and increasing the reactivity of the cement, corroborating the results from Vicat indentation. The pH curves obtained in this work presented similar behavior from those presented by Canal et al. [34], and TenHuisen and Brown [33], however, punctual values are different as particle size of α-TCP used in their works are below the 5.0 μm and applied thermal treatments granted them higher reactivity. Finally, the stabilization pH after 48 h of reaction was of 6.91 for C0, 5.46 for C10, 5.56 for C15 and 5.57 for C15, indicating that the more acidic character remains in conditions with HAC-B added, nevertheless, within the range of CDHA precipitation.

XRF

The Ca/P molar ratio present in each CPC formulation after setting is presented in Table 3. From these results, it is possible to establish that the variations of CHA-B addition do not cause significant changes to the Ca/P molar ratio of CPCs, which can be attributed to the fact that these additions are considered low compared to the amount of material used during the test, as stated before, its function is to act as a nucleating agent. Thus, it is corroborated that the Ca/P molar ratio in CPC is mainly governed by the chemical composition of the α-TCP [48].

Values close to 1.5 is characteristic of CDHA, indicating that the obtained cements have appropriate chemical conditions to be used as bone implants as they are within the range of natural bones [48].

FTIR

For all the CPCs produced, the wave number ranges between 1600–400 cm^{-1} and 3700–3000 cm^{-1} were selected to verify the existence of the functional groups characteristic of CDHA present in the obtained cements. Fig. 5 illustrates the FTIR spectra of all the CPC formulations with different CHA-B additions. Besides, an insert is presented for the analysis of the vibrations corresponding to OH^-. The four spectra similarity indicates that there are no evident changes due to the addition of CHA-B and that the characteristic spectrum of CDHA is obtained in all conditions.

The acquired spectra present four characteristic vibration modes of the PO_4^{3-} ion: ν_1 at 956 cm^{-1} of the symmetric P–O stretching, ν_2 at 415–470 cm^{-1} of the symmetric double degenerated P–O rolling, ν_3 at 984–1058 cm^{-1} of the antisymmetric triple degenerated P–O stretching and ν_4 at 551–613 cm^{-1} of the antisymmetric triple degenerated P–O rolling. Besides, two types of vibrations are presented for the OH^- ion: ν_s at 3572 cm^{-1}, a weak peak that corresponds to the stretching of the hydroxyl group and ν_L at 630 cm^{-1}, which confirm us that the setting has been successful to obtain a hydroxyapatite; in addition, it is observed a wide absorption at 870 cm^{-1} that corresponds to the stretching mode P–O (H) of HPO_4^{2-} group,

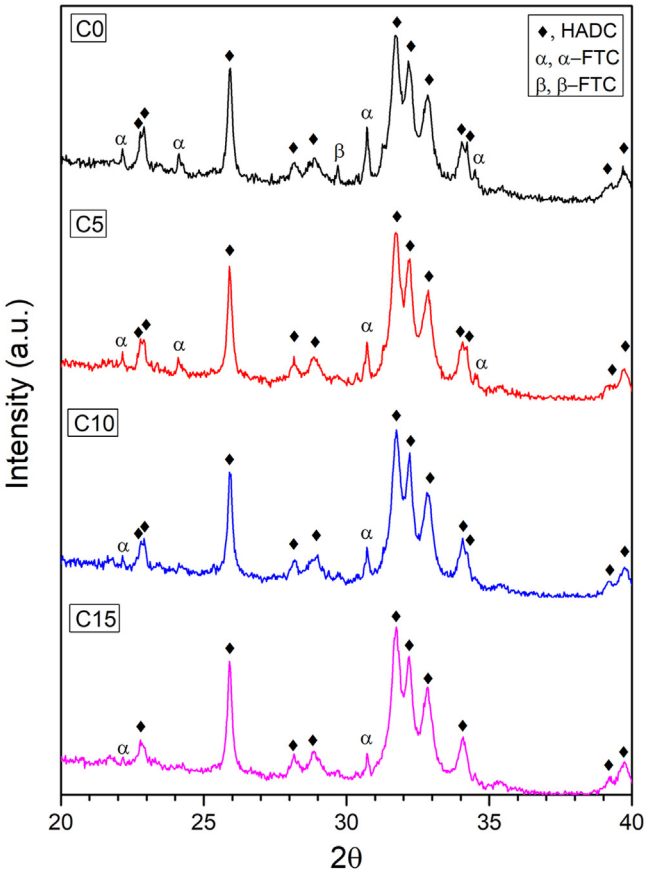

Fig. 6 – X-ray diffractograms of CPCs as a function of the percentage of CHA-B added. Diffraction patterns 09-0348: α-TCP; 09-0169: β-TCP; 46-905: CDHA.

which indicates a calcium deficiency in the obtained cement [49].

The peak of the carbonate ion is not evidenced in any of the obtained cements, being possible that during the immersion in NaCl solution, for the setting process, CO_3 has diffused.

XRD

The X-ray diffraction patterns of the cement formulations are shown in Fig. 6. The peaks obtained were identified by means of the JCPDS 46-905 reference standard for CDHA, which indicates that the setting conditions are adequate to promote the dissolution process of α-TCP and subsequent precipitation of the CDHA phase, however, the reaction requires more time since some peaks corresponding to the α- TCP and β-TCP phases remain, perhaps, due to large particles of the alpha polymorph that do not manage to fully react during setting and to the low solubility of the beta phase [11,49].

It is clearly seen how the intensity of the peaks located at 22.16°; 24.13°; 30.71° and 34.51° for the α-TCP remnant and the peak located at 29.70° for the β-TCP remnant decrease to almost disappear as CHA-B addition increases. This behavior can be attributed to CHA-B acting as a nucleant agent for the CDHA phase. In order to corroborate this tendency, a phase quantification analysis was carried out applying Rietveld's methodology. The results are presented in Table 4 where the

Table 4 – Percentage by weight of phases present in CPCs set at 37 °C for 7 days in Ringer solution.

Cement formulation	CDHA	α-TCP	β-TCP
C0	79.8 ± 0.1	16.4 ± 0.8	3.8 ± 0.4
C5	84.2 ± 0.1	10.5 ± 0.5	5.4 ± 0.5
C10	90.9 ± 0.1	6.8 ± 0.5	2.2 ± 0.4
C15	93.0 ± 0.1	5.8 ± 0.4	1.2 ± 0.4

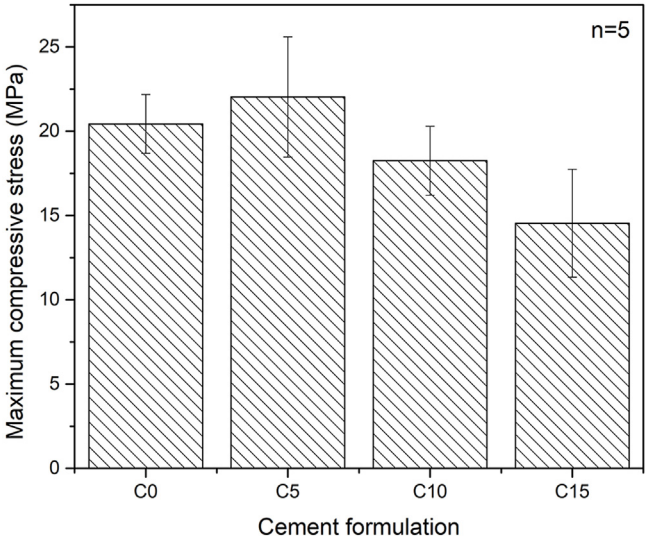

Fig. 7 – Maximum compressive strength of CPCs, (*n* = number of replicates).

CDHA phase content progressively increases as a function of CHA-B addition, which confirms the action as nucleation agent. These results hint that all tested CPC would present good *in vivo* performance related to the elevated CDHA content [15,50].

Maximum axial compressive strength

Fig. 7 shows the maximum axial compressive strength of the various conditions tested. An influence of the percentage of addiction of CHA-B is difficult to determine as the only condition that present a significative difference is C15. It can be seen that the formulation with 5% in weight of CHA-B addition, presents a slight increase in the maximum resistance compared with the cement without modifications, changing from 20.4 ± 1.8 MPa for C0 to 22.0 ± 3.6 MPa for C5. Although, according to the deviations obtained in the results, the difference is not significant. It is possible that the slight increase is related to the nucleating effect of CHA-B for the CDHA phase, since the mechanical properties are directly related to the greater quantity and entanglement of CDHA crystals [21]. However, for the conditions of higher percentage of CHA-B addition (*i.e.* C10 and C15), values of 18.3 ± 2.0 MPa and 14.5 ± 3.2 MPa are obtained respectively, which does not agree with the higher amount of CDHA, as presented in Table 4. This is attributed to the possible CHA-B agglomerates that may be formed in CPCs due to the nanometric character of the CHA-B particles that could act as stress concentrators.

CPCs may present compressive strength as high as 80 MPa, depending on the compaction of the sample, the particle size

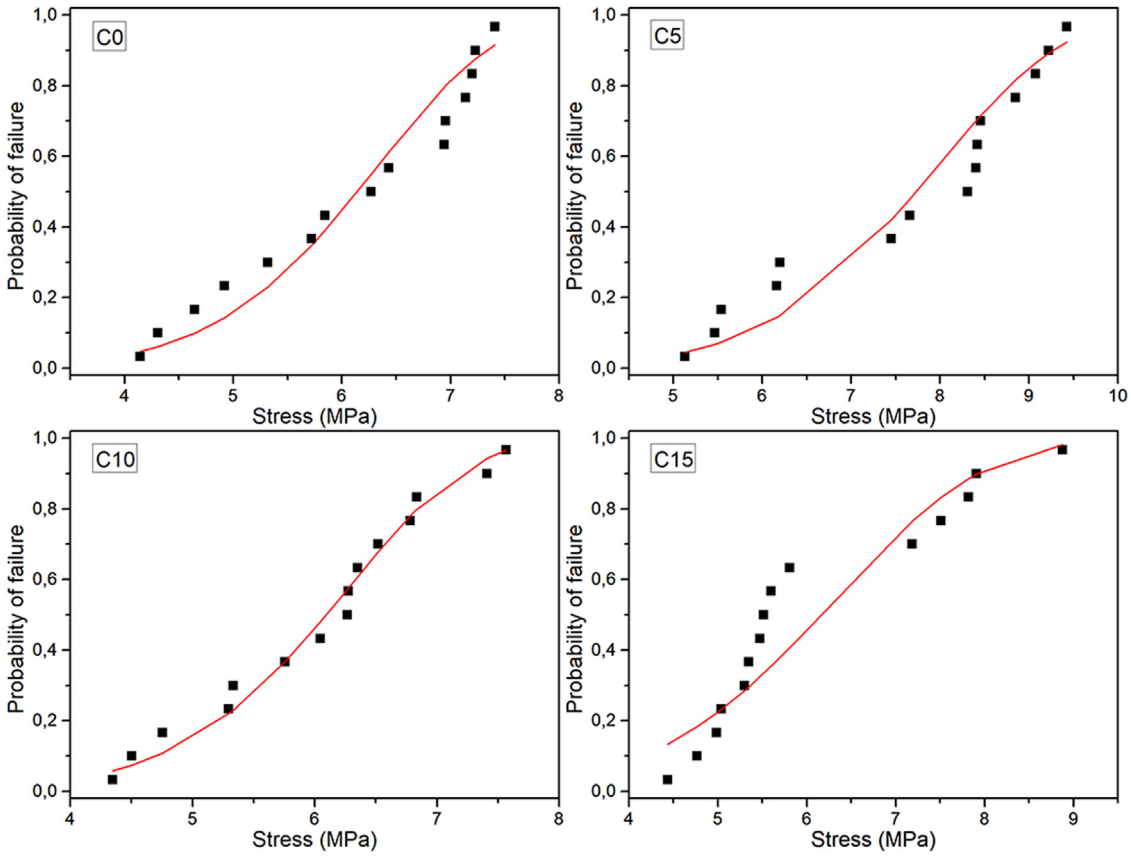

Fig. 8 – Graphs of Weibull distributions of formulated CPCs. Squares: experimental values (Eq. (2)). Red lines: P_f calculated using the Weibull module and the characteristic stress values of Table 5.

of the precursors or the L/P ratio [51,52]. Although the porosity of the samples was not measured, comparison can be made with similar CPC prepared by Espanol et al. [19], where coarse α-TCP with a slight lower median particle size of 5.5 μm and broader distribution (0.1–40 μm), suggest that our prepared CPCs may present porosity values between 25 and 35% for L/P of 0.44 mL/g. In addition, the compressive strength ranged from 28 to 38 MPa, suggesting that the bigger particle size of α-TCP obtained in this work is the major responsible of the slight lower compressive strength.

Table 5 – Parameters of Weibull distributions, characteristic strength (σ_0), Weibull modulus (m) and 10, 50 and 90% probability of failure for each condition.

Cement formulation	σ_0 (MPa)	m	P_f – 10%	P_f – 50%	P_f – 90%
C0	6.48	6.78	4.64	6.13	7.34
C5	8.17	6.61	5.8	7.74	9.29
C10	6.41	7.29	4.71	6.1	7.24
C15	6.65	4.80	4.45	6.17	7.91

Maximum diametrical stress resistance

Based on the results and calculations of the Weibull distribution, it was constructed Fig. 8, where the dotted values correspond to the experimental data and were determined using Eq. (2), while continuous lines correspond to the Weibull probability plots based on Eq. (3).

Table 5 compiles the Weibull parameters and the characteristic stress associated with the 10, 50 and 90% probability of failure for each cement sample. It is possible to see that the characteristic strength and probabilities are greater for the 5% CHA-B sample. This result that agrees with the observed tendency in axial compression, attributed to the fact that there can be an effect of CHA-B addition in terms of larger nucleation points for the precipitation of the CDHA phase. The other conditions show similar values to condition without CHA-B addition, which, as explained before, can be caused by the formed agglomerates.

The Weibull modulus variation indicates that higher value is obtained for C10 (m = 7.29) and lower for C15 (m = 4.80) which indicates that these conditions are the most and less reliable values, respectively. Both C0 and C5 present similar modulus indicating that both conditions are equally reliable. The low m value of C15 propose that the defects present in the cement are more gathered in comparison with the other cements [53]. Result that, once again, is attributed to the possibility of higher agglomerations due to the higher amount of CHA-B.

The diametral tensile strength of the cements may be considered higher than others reported [43,54,55], which may be attributed to the longer setting time here used. Nevertheless, Baudin et al. [30] used similar setting process (24 h room temperature + 7 days at 36.5 °C) and differences related to the

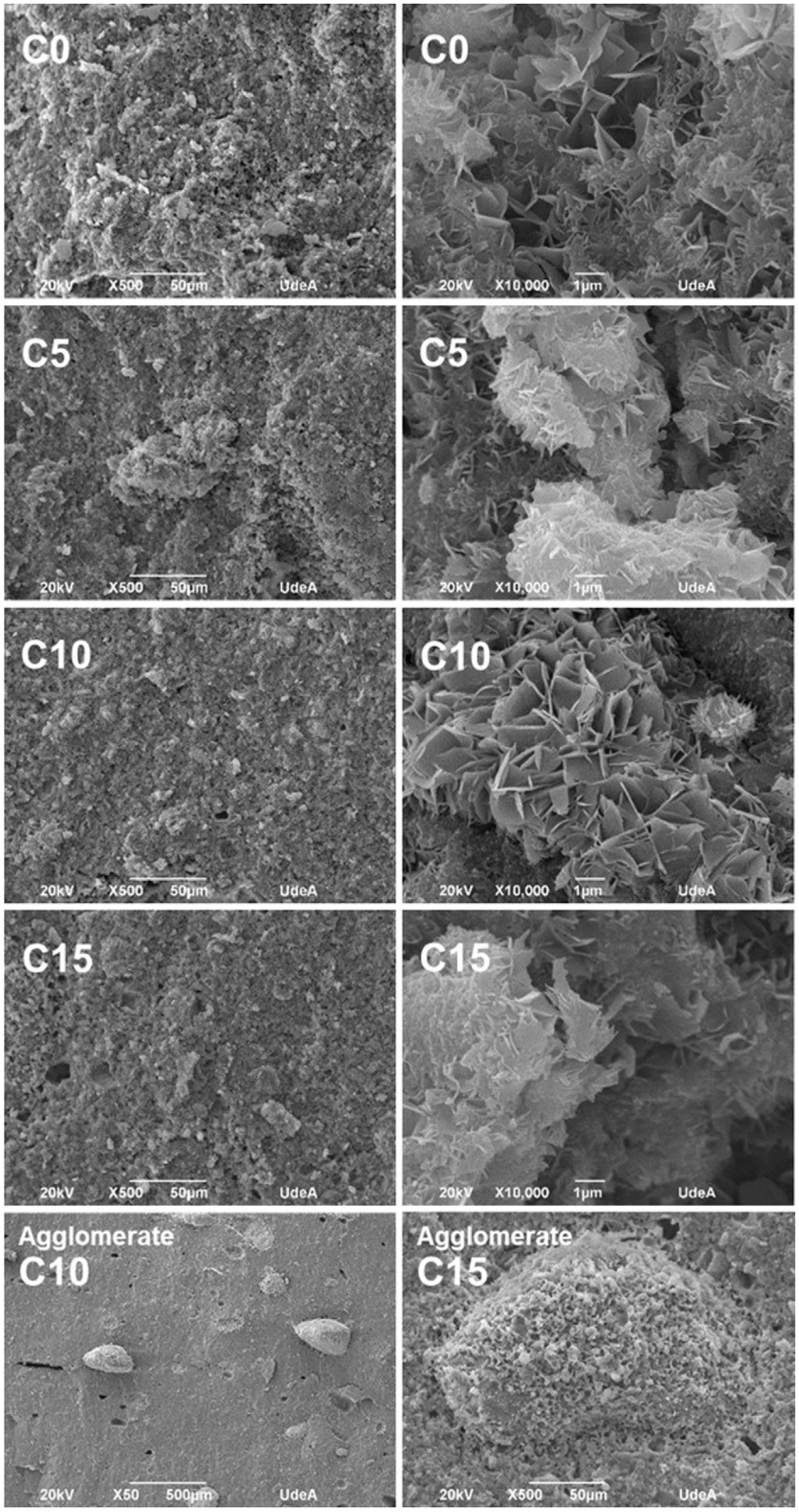

Fig. 9 – SEM micrographs of the fracture surface of each CPC formulation; 500× and 10 000× from left to right for C0, C5 C10 and C15 (from top to bottom). Final row show agglomerates present in C10 and C15 samples.

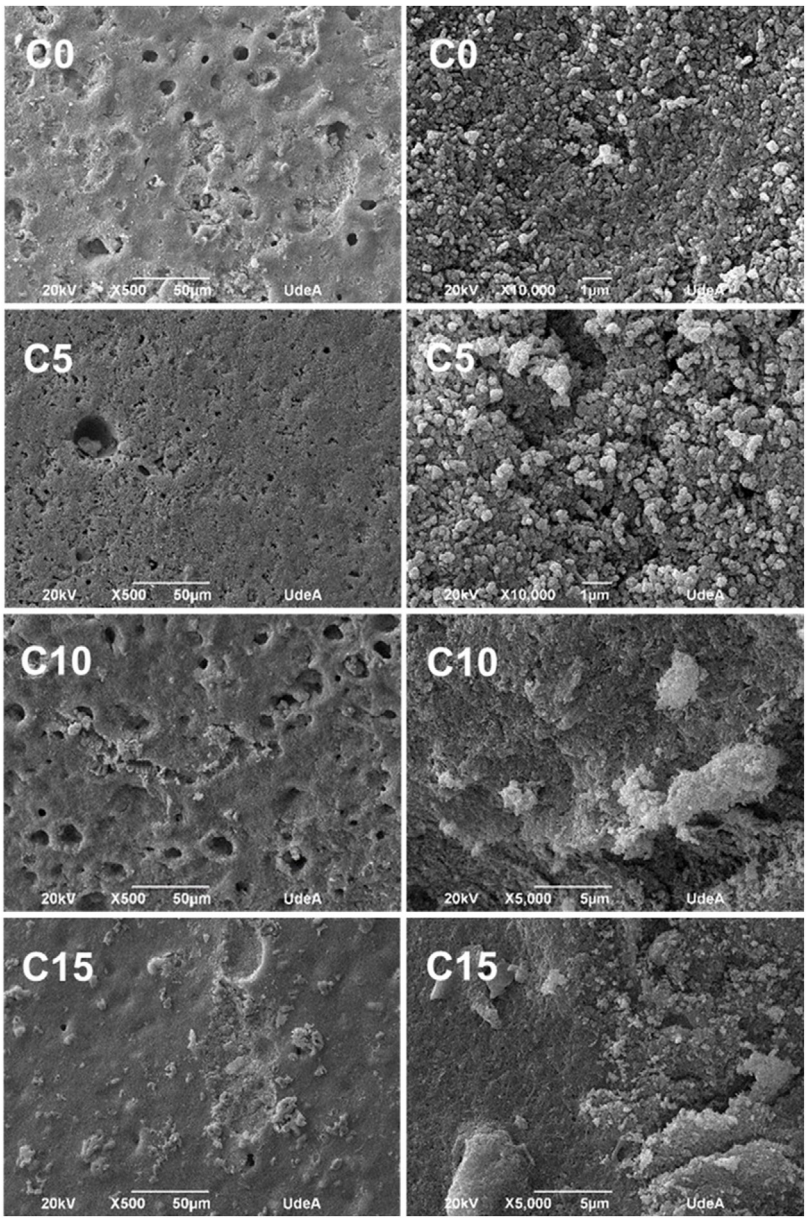

Fig. 10 – SEM micrographs of the surface exposed to pH equal to 2; 500× and 10 000× from left to right for C0, C5 C10 and C15 (from top to bottom).

pristine cement may be attributed to the lower amount of CDHA and higher L/P ratio than the ones here presented.

Morphology of CPCs

Fig. 9 shows SEM micrographs of all CPC formulations. At low magnifications, it can be seen a porous and rough surface, suitable to favor the osteoconduction at *in vivo* level; while at higher magnifications, it is possible to distinguish the characteristic flower structure of CDHA crystals in CPCs, where the flower is an agglomerate of CDHA crystals that share a nucleation point. It is also possible to appreciate the entanglement of the crystals, important to have high mechanical resistance [5,21]. All the formulations presented these characteristics, so together with the results of FTIR and XRD it can be inferred that the setting process, although not complete, is adequate to obtain a CPC with CDHA crystals properly organized which give place to a stable structure.

In conditions C10 and C15 it was detected large agglomerates attributed to CHA-B (Fig. 8, bottom images). In C10 agglomerates were of approximately 350 µm and in C15 of 195 µm. Agglomerates are attributed to the nanometric size of CHA-B and may be acting as stress concentrators.

It was expected that the higher CDHA content in C10 and C15 would lead to higher mechanical resistance, although, observed agglomerations promoted equal or lower mechanical resistance by increment of CHA-B in CPCs, indicating that the presence of these defects have higher effect in the final mechanical resistance. In C5 it was not observed such high agglomerates, assuming that CHA-B has been better

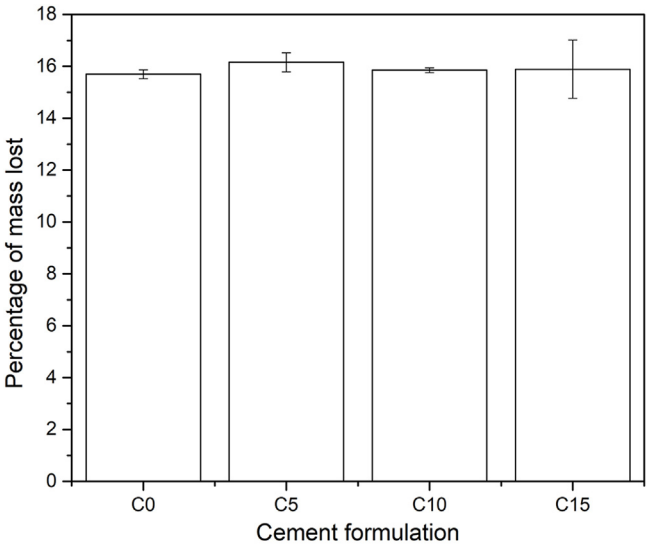

Fig. 11 – Percentage mass loss of CPCs after accelerated degradation test at pH 2, 37 °C and 100 RPM for 8 h.

distributed in the cement, promoting the tendency toward a higher mechanical resistance.

Accelerated degradation test

Fig. 10 shows SEM micrographs of samples from the accelerated degradation test. For the images at lower magnification, a smooth surface is observed, and at higher magnifications the microstructural changes of the cements are noticeable, since the characteristic crystals of CDHA shown in Fig. 9 have been dissolved by the acid solution (pH = 2) used during the test [36]. These results are adequate as they indicate that CPCs will have a biodegradable character under *in vivo* conditions regardless of the added percentage of CHA-B.

In addition, the pH of the solution in each of the containers was measured every hour, where it was obtained that this fluctuated between values of 1.97 and 2.03 on the pH scale, indicating that during the 8 h of duration of the test the acidity remained constant. Finally, at the end of the degradation test, the change in mass of each specimen was calculated; the results are shown in Fig. 11. All the conditions presented a loss of mass around 16% in weight, which indicates that the addition of CHA-B maintains the biodegradable character of calcium phosphate cements suitable for bone implants. Likewise, it is to be appreciated that the C15 data present a greater dispersion, attributed to the fact that CHA-B exhibits a higher reactivity character, and when presenting a greater content of it, it causes a greater fluctuation in the data.

Conclusions

In this study, carbonate hydroxyapatite type B seemed to be obtained by inverse aqueous reaction method and calcium phosphate cements with different additions of this HAC-B were developed. Cements showed to be suitable for bone substitutes due to its chemical composition, high presence of calcium-deficient hydroxyapatite and the appropriate mechanical resistance which are similar to the ones presented in trabecular bone. The FTIR result was consistent with XRD, SEM and the calculated Ca/P ratio, confirming the formation of CDHA in all experimented formulation. Besides, by means of diffractograms and phase analysis by Rietveld method, it was appreciated that the addition of carbonated hydroxyapatite type B decreases the amount of residual α and β tricalcium phosphate in the final CPC. It was identified that the condition that has 5% in weight of carbonated hydroxyapatite type B tends to have a higher mechanical response especially in diametral strength, but higher additions decreases to values close to the one showed by the cement without additives.

In this work we have demonstrated that the CHA-B addition acts as a nucleant agent to obtain CDHA in calcium phosphate cements, improving its properties with a good *in vitro* behavior.

Acknowledgements

The authors would like to thank the Colombian Ministry of Science, Technology and Innovation (MINCIENCIAS) for the funds granted to project 1115745-57862, contract 012-2017 and the Young Researchers Program from the University of Antioquia for the internship in the ceramic materials and coatings research group (GIMACYR).

REFERENCES

[1] E. Champion, Sintering of calcium phosphate bioceramics, Acta Biomater. 9 (2013) 5855–5875, http://dx.doi.org/10.1016/j.actbio.2012.11.029.
[2] S. Dorozhkin, Calcium orthophosphate-based bioceramics, Materials (Basel) 6 (2013) 3840–3942, http://dx.doi.org/10.3390/ma6093840.
[3] S.B.H. Farid, Hard tissue engineering applications, Bioceram. Mater. Sci. Eng. (2019) 119–158, http://dx.doi.org/10.1016/B978-0-08-102233-7.00005-7.
[4] N.W. Kucko, R.-P. Herber, S.C.G. Leeuwenburgh, J.A. Jansen, Calcium phosphate bioceramics and cements, Princ. Regen. Med. (2018) 591–611, http://dx.doi.org/10.1016/b978-0-12-809880-6.00034-5.
[5] S. Dorozhkin, Self-setting calcium orthophosphate formulations, J. Funct. Biomater. 4 (2013) 209–311, http://dx.doi.org/10.3390/jfb4040209.
[6] Organización mundial de la salud, Discapacidad y salud, 2018.
[7] S.V. Dorozhkin, Calcium-orthophosphate-based bioactive ceramics, Fundam. Biomater. Ceram. (2018) 297–405, http://dx.doi.org/10.1016/B978-0-08-102203-0.00013-5.
[8] S. Oh, N. Oh, M. Appleford, J.L. Ong, Bioceramics for tissue engineering applications "a review", Am. J. Biochem. Biotechnol. 2 (2006) 49–56, http://dx.doi.org/10.3844/ajbbsp.2006.49.56.
[9] D. Apelt, F. Theiss, A.O. El-Warrak, K. Zlinszky, R. Bettschart-Wolfisberger, M. Bohner, S. Matter, J.A. Auer, B. Von Rechenberg, In vivo behavior of three different injectable hydraulic calcium phosphate cements, Biomaterials 25 (2004) 1439–1451, http://dx.doi.org/10.1016/j.biomaterials.2003.08.073.
[10] R.G. Carrodeguas, S. De Aza, α-Tricalcium phosphate: synthesis, properties and biomedical applications, Acta Biomater. 7 (2011) 3536–3546, http://dx.doi.org/10.1016/j.actbio.2011.06.019.
[11] D. Moreno, F. Vargas, J. Ruiz, M.E. López, Solid-state synthesis of alpha tricalcium phosphate for cements used in

biomedical applications, Bol. Soc. Españ. Cerám. Vidr. 59 (2020) 193–200, http://dx.doi.org/10.1016/j.bsecv.2019.11.004.
[12] N. Eliaz, N. Metoki, Calcium phosphate bioceramics: a review of their history, structure, properties, coating technologies and biomedical applications, Materials (Basel) 10 (2017) 334, http://dx.doi.org/10.3390/ma10040334.
[13] C. Canal, S. Gallinetti, M.P. Ginebra, Low-pressure plasma treatment of polylactide fibers for enhanced mechanical performance of fiber-reinforced calcium phosphate cements, Plasma Process. Polym. 11 (2014) 694–703, http://dx.doi.org/10.1002/ppap.201400018.
[14] A. Barba, A. Diez-Escudero, Y. Maazouz, K. Rappe, M. Espanol, E.B. Montufar, M. Bonany, J.M. Sadowska, J. Guillem-Marti, C. Öhman-Mägi, C. Persson, M.-C. Manzanares, J. Franch, M.-P. Ginebra, Osteoinduction by foamed and 3D-printed calcium phosphate scaffolds: effect of nanostructure and pore architecture, ACS Appl. Mater. Interf. 9 (2017) 41722–41736, http://dx.doi.org/10.1021/acsami.7b14175.
[15] A. Barba, Y. Maazouz, A. Diez-Escudero, K. Rappe, M. Espanol, E.B. Montufar, C. Öhman-Mägi, C. Persson, P. Fontecha, M.-C. Manzanares, J. Franch, M.-P. Ginebra, Osteogenesis by foamed and 3D-printed nanostructured calcium phosphate scaffolds: effect of pore architecture, Acta Biomater. 79 (2018) 135–147, http://dx.doi.org/10.1016/j.actbio.2018.09.003.
[16] S. Gallinetti, G. Mestres, C. Canal, C. Persson, M.-P. Ginebra, A novel strategy to enhance interfacial adhesion in fiber-reinforced calcium phosphate cement, J. Mech. Behav. Biomed. Mater. 75 (2017) 495–503, http://dx.doi.org/10.1016/j.jmbbm.2017.08.017.
[17] J.P. Schmitz, J.O. Hollinger, S.B. Milam, Reconstruction of bone using calcium phosphate bone cements: a critical review, J. Oral Maxillofac. Surg. 57 (1999) 1122–1126, http://dx.doi.org/10.1016/S0278-2391(99)90338-5.
[18] L.L. Hench, Bioceramics: from concept to clinic, J. Am. Ceram. Soc. 74 (1991) 1487–1510, http://dx.doi.org/10.1111/j.1151-2916.1991.tb07132.x.
[19] M. Espanol, R.A. Perez, E.B. Montufar, C. Marichal, A. Sacco, M.P. Ginebra, Intrinsic porosity of calcium phosphate cements and its significance for drug delivery and tissue engineering applications, Acta Biomater. 5 (2009) 2752–2762, http://dx.doi.org/10.1016/j.actbio.2009.03.011.
[20] A.M.C. Barradas, H. Yuan, J. van der Stok, B. Le Quang, H. Fernandes, A. Chaterjea, M.C.H. Hogenes, K. Shultz, L.R. Donahue, C. van Blitterswijk, J. de Boer, The influence of genetic factors on the osteoinductive potential of calcium phosphate ceramics in mice, Biomaterials 33 (2012) 5696–5705, http://dx.doi.org/10.1016/j.biomaterials.2012.04.021.
[21] M.P. Ginebra, C. Canal, M. Espanol, D. Pastorino, E.B. Montufar, Calcium phosphate cements as drug delivery materials, Adv. Drug Deliv. Rev. 64 (2012) 1090–1110, http://dx.doi.org/10.1016/j.addr.2012.01.008.
[22] F.C.M. Driessens, The mineral in bone, dentin and tooth enamel, Bull. Des. Soc. Chim. Belges. 89 (2010) 663–689, http://dx.doi.org/10.1002/bscb.19800890811.
[23] D. Tadic, F. Peters, M. Epple, Continuous synthesis of amorphous carbonated apatites, Biomaterials 23 (2002) 2553–2559, http://dx.doi.org/10.1016/S0142-9612(01)00390-8.
[24] M. Canillas, P. Pena, A. De Aza, M.A. Rodríguez, Calcium phosphates for biomedical applications, Bol. Soc. Españ. Cerám. Vidr. 6 (2017) 1–22, http://dx.doi.org/10.1016/j.bsecv.2017.05.001.
[25] J.-P. Lafon, Synthèse, stabilité thermique et frittage d'hydroxyapatites carbonatées, 2004.
[26] Y. Botero, Hidroxiapatita carbonatada, una opción como biomaterial para implantes: una revisión del estado del arte, Rev. Colomb. Mater. (2016) 79–97.
[27] D. Moreno, F. Vargas, E. López, Efecto de la relación líquido a polvo en las propiedades fisicoquímicas de cementos de fosfato de calcio y de estos sobre el espesor de Biofilm de *Staphylococcus aureus* adherido (Effect of the liquid-to-powder ratio on physicochemical properties of calcium phosphate cements and of these properties over Biofilm thickness of adhered *Staphylococcus aureus*), DYNA 88 (2021) 102–110, http://dx.doi.org/10.15446/dyna.v88n219.93812.
[28] R.G. Carrodeguas, A.H. De Aza, X. Turrillas, P. Pena, S. De Aza, New approach to the β→α polymorphic transformation in magnesium-substituted tricalcium phosphate and its practical implications, J. Am. Ceram. Soc. 91 (2008) 1281–1286, http://dx.doi.org/10.1111/j.1551-2916.2008.02294.x.
[29] Astm C1424-15, standard test method for monotonic equibiaxial flexural strength of advanced ceramics at ambient temperature 1, ASTM Stand. 3 (2009) 1–13, http://dx.doi.org/10.1520/C1499-09.
[30] C. Baudín, T. Benet, P. Pena, Effect of graphene on setting and mechanical behaviour of tricalcium phosphate bioactive cements, J. Mech. Behav. Biomed. Mater. 89 (2019) 33–47, http://dx.doi.org/10.1016/j.jmbbm.2018.09.002.
[31] American Society for Testing and Materials, Standard test method for time of setting of hydraulic cement by vicat needle ASTM C191-13, ASTM Stand. B (2013), http://dx.doi.org/10.1520/C0191-13.2.
[32] J. Weichhold, U. Gbureck, F. Goetz-Neunhoeffer, K. Hurle, Setting mechanism of a CDHA forming α-TCP cement modified with sodium phytate for improved injectability, Materials (Basel) 12 (2019), http://dx.doi.org/10.3390/ma12132098.
[33] K.S. TenHuisen, P.W. Brown, Formation of calcium-deficient hydroxyapatite from α-tricalcium phosphate, Biomaterials 19 (1998) 2209–2217, http://dx.doi.org/10.1016/S0142-9612(98)00131-8.
[34] C. Canal, D. Pastorino, G. Mestres, P. Schuler, M.P. Ginebra, Relevance of microstructure for the early antibiotic release of fresh and pre-set calcium phosphate cements, Acta Biomater. 9 (2013) 8403–8412, http://dx.doi.org/10.1016/j.actbio.2013.05.016.
[35] M. Ferrari, L. Lutterotti, Method for the simultaneous determination of anisotropic residual stresses and texture by X-ray diffraction, J. Appl. Phys. 76 (1994) 7246–7255.
[36] A. Diez-Escudero, M. Espanol, S. Beats, M.P. Ginebra, In vitro degradation of calcium phosphates: effect of multiscale porosity, textural properties and composition, Acta Biomater. 60 (2017) 81–92, http://dx.doi.org/10.1016/j.actbio.2017.07.033.
[37] E. Landi, G. Celotti, G. Logroscino, A. Tampieri, Carbonated hydroxyapatite as bone substitute, J. Eur. Ceram. Soc. 23 (2003) 2931–2937, http://dx.doi.org/10.1016/S0955-2219(03)00304-2.
[38] C. Ortali, I. Julien, M. Vandenhende, C. Drouet, E. Champion, Consolidation of bone-like apatite bioceramics by spark plasma sintering of amorphous carbonated calcium phosphate at very low temperature, J. Eur. Ceram. Soc. 38 (2018) 2098–2109, http://dx.doi.org/10.1016/j.jeurceramsoc.2017.11.051.
[39] H. Madupalli, B. Pavan, M.M.J. Tecklenburg, Carbonate substitution in the mineral component of bone: discriminating the structural changes, simultaneously imposed by carbonate in A and B sites of apatite, J. Solid State Chem. 255 (2017) 27–35, http://dx.doi.org/10.1016/j.jssc.2017.07.025.
[40] W. Liu, D. Zhai, Z. Huan, C. Wu, J. Chang, Novel tricalcium silicate/magnesium phosphate composite bone cement having high compressive strength, in vitro bioactivity and cytocompatibility, Acta Biomater. 21 (2015) 217–227, http://dx.doi.org/10.1016/j.actbio.2015.04.012.

[41] S. Jegou Saint-Jean, C.L. Camiré, P. Nevsten, S. Hansen, M.P. Ginebra, Study of the reactivity and in vitro bioactivity of Sr-substituted α-TCP cements, J. Mater. Sci. Mater. Med. 16 (2005) 993–1001, http://dx.doi.org/10.1007/s10856-005-4754-z.
[42] D. Pastorino, C. Canal, M.-P. Ginebra, Multiple characterization study on porosity and pore structure of calcium phosphate cements, Acta Biomater. 28 (2015) 205–214, http://dx.doi.org/10.1016/j.actbio.2015.09.017.
[43] C. Durucan, P.W. Brown, Reactivity of α-tricalcium phosphate, J. Mater. Sci. 37 (2002) 963–969, https://doi.org/https://doi-org.recursos.biblioteca.upc.edu/10.1023/A:1014347814241.
[44] M. Bohner, Reactivity of calcium phosphate cements, 2007, pp. 3980–3986, http://dx.doi.org/10.1039/b706411j.
[45] F.C.M. Driessens, O. Bermúdez, M.G. Boltong, J.A. Planell Estany, Desarrollo de nuevos cementos óseos a base de fosfato de calcio: resumen de un estudio piloto, Biomecánica 2 (1994), http://dx.doi.org/10.5821/sibb.v2i2.1562.
[46] C. Liu, H. Shao, F. Chen, H. Zheng, Rheological properties of concentrated aqueous injectable calcium phosphate cement slurry, Biomaterials 27 (2006) 5003–5013, http://dx.doi.org/10.1016/j.biomaterials.2006.05.043.
[47] J. Liu, J. Li, J. Ye, F. He, Setting behavior, mechanical property and biocompatibility of anti-washout wollastonite/calcium phosphate composite cement, Ceram. Int. 42 (2016) 13670–13681, http://dx.doi.org/10.1016/j.ceramint.2016.05.165.
[48] E.I. Dorozhkina, S.V. Dorozhkin, Mechanism of the solid-state transformation of a calcium-deficient hydroxyapatite (CDHA) into biphasic calcium phosphate (BCP) at elevated temperatures, Chem. Mater. 14 (2002) 4267–4272, http://dx.doi.org/10.1021/cm0203060.
[49] I. Grigoraviciute-Puroniene, Y. Tanaka, V. Vegelyte, Y. Nishimoto, K. Ishikawa, A. Kareiva, A novel synthetic approach to low-crystallinity calcium deficient hydroxyapatite, Ceram. Int. 45 (2019) 15620–15623, http://dx.doi.org/10.1016/j.ceramint.2019.05.072.
[50] N.W. Kucko, S. de Lacerda Schickert, T. Sobral Marques, R.-P. Herber, J.J. van den Beucken, Y. ZUO, S.C.G. Leeuwenburgh, Tough and osteocompatible calcium phosphate cements reinforced with poly(vinyl alcohol) fibers, ACS Biomater. Sci. Eng. (2019), http://dx.doi.org/10.1021/acsbiomaterials.9b00226.
[51] M. Geffers, J. Groll, U. Gbureck, Reinforcement strategies for load-bearing calcium phosphate biocements, Materials (Basel) 8 (2015) 2700–2717, http://dx.doi.org/10.3390/ma8052700.
[52] U. Gbureck, K. Spatz, R. Thull, J.E. Barralet, Rheological enhancement of mechanically activated α-tricalcium phosphate cements, J. Biomed. Mater. Res. - Part B: Appl. Biomater. 73 (2005) 1–6, http://dx.doi.org/10.1002/jbm.b.30148.
[53] S. Raymond, Y. Maazouz, E.B. Montufar, R.A. Perez, B. González, J. Konka, J. Kaiser, M.-P. Ginebra, Accelerated hardening of nanotextured 3D-plotted self-setting calcium phosphate inks, Acta Biomater. 75 (2018) 451–462, http://dx.doi.org/10.1016/j.actbio.2018.05.042.
[54] E. Fujihara, M. Kon, K. Asaoka, Strontium-substituted calcium phosphate cements prepared with strontium-containing solutions, Key Eng. Mater. 330–332 (2007) 795–798, http://dx.doi.org/10.4028/www.scientific.net/kem.330-332.795.
[55] C.-H. David Chen, C.-C. Chen, M.-Y. Shie, C.-H. Huang, S.-J. Ding, Controlled release of gentamicin from calcium phosphate/alginate bone cement, Mater. Sci. Eng. C 31 (2011) 334–341, http://dx.doi.org/10.1016/j.msec.2010.10.002.